Near-Field Intra-body Optical Communication: Leveraging the Power of Bessel Beams

Hadeel Elayan and Josep Jornet
Institute for the Wireless Internet of Things, Northeastern University, Boston, U.S.A
h.mohammad@northeastern.edu, j.jornet@northeastern.edu

***Abstract*—This work explores the use of Bessel beams as a potential solution for near-field optical intra-body communication. Bessel beams possess unique non-diffracting and self-healing properties, making them superior to traditional Gaussian beams in maintaining intensity through complex biological environments in the near-field. In this paper, we propose a system that employs optical nanoantenna arrays to generate Bessel beams at a wavelength of 1550 nm, which falls within the biological transparency window. The system model is described, including its design principles and the corresponding mathematical formulation. Our results compare the propagation characteristics of Bessel and Gaussian beams in intra-body contexts, highlighting the role of near-field effects in ensuring propagation stability and preserving beam integrity at cellular levels.**

***Index Terms*—Bessel beams, intra-body, optical communication, near-field.**

I. Introduction

Over the past decade, as the field of nanonetworking has advanced, plasmonic nanoantennas have emerged as key enablers, pushing the boundaries of communication at the nanoscale [1]. By focusing light beyond the diffraction limit, these nanoantennas enable highly localized and efficient interplay between nanoscale devices. This capability has opened new avenues in photonics, facilitating precise control of light-matter interactions [2]. Structural optimizations, such as adjusting gap size, refining antenna dimensions and shape, and organizing them into arrays, have significantly enhanced field concentration and enabled precise tuning of the antenna's spectral response [3]. In particular, nanoantenna arrays have proven to be highly valuable for controlling light-matter interactions by leveraging collective electromagnetic (EM) resonances.

Nanofabrication is essential for harnessing these interactions, as it enables the precise design of nanoantenna arrays. A wide variety of structures have been synthesized and characterized, with plasmon resonances tunable across the visible to mid-infrared range of the EM spectrum [4]. The geometry and material properties of these arrays directly shape the phase and amplitude distribution of the electric field, facilitating the tailored manipulation of wavefronts, which connect points of a wave oscillating in unison. Wavefront shaping provides a powerful technique for enhancing optical resolution in focusing and imaging by mitigating the challenges caused by the exponential decay of ballistic photons—light particles that traverse a medium without scattering. This approach enables micrometer or even sub-micrometer resolution deep within complex media, allowing the retrieval of information from scattered light [5]. Therefore, understanding and controlling the wavefront is crucial for optimizing the performance of nanoantenna systems across various applications, particularly in complex environments.

By applying the same principles as radio frequency (RF) antennas, optical nanoantennas can operate wirelessly, paving the way for *in-vivo* nano-bio sensing and actuation [6]. Nanoscale communication has emerged as a promising field, enabling interactions between nanomachines within the body or between implanted nanomachines and wearable devices. For such communication, various technologies have been proposed, with optical frequency bands—such as infrared (30-400 THz) and visible light (400-750 THz)—standing out as effective solutions for nanoscale connectivity [7]. To improve the range of wireless communication for deeper implants, the work in [8] proposed combining analog beamforming with optical nanoantenna arrays and light-guiding hydrogel implants to counteract propagation losses and extend communication distance within the body.

A key consideration in these systems is achieving precise control and high spatial resolution, where near-field effects become essential for enhanced communication at microscopic scales. Unlike conventional beamforming solutions, which typically produce Gaussian beams, the near-field enables advanced design options such as beamfocusing, curved Airy beams, and Bessel beams [9]. In particular, Bessel beams stand out due to their ability to maintain a non-diffracting profile over longer distances compared to Gaussian beams [10], making them ideal for intra-body optical communications. Those beams have already been applied in various fields, including optical tweezers [11], optical coherence tomography [12], and free-space optical communication [13]. Recently, they have been proposed for near-field terahertz (THz) communication [14].

In this paper, we present Bessel beams as a solution for near-field optical intra-body communications. Our work paves the way for the development of a new generation of devices that harness near-field behavior for unprecedented precision in nanonetworks. This opens new possibilities for innovations in sensing and actuation, setting the stage for advancements in optical nano-communication. To this end, we summarize our contributions as follows

- We introduce the concept of near-field optical communication within the body.

- We present Bessel beams as a promising approach to enhancing intra-body communication, detailing the system design and its corresponding mathematical analysis.

The remainder of the paper is structured as follows. In Sec. II, we explore the principles underlying near-field intra-body communication. Sec. III introduces Bessel beams as a new approach for intra-body communication, presenting both the proposed system and its mathematical formulation. In Sec. IV, we demonstrate the results derived from our developed model. Finally, we conclude our findings in Sec. V.

II. Near-Field Analysis

A. Physical Basis

The Fraunhofer distance defines the boundary between the near-field and far-field, representing the point beyond which diffraction effects dominate and the beam propagates in a well-defined, collimated manner [15]. In our work, this distance becomes especially important when the effective dimension of the nanoantenna array exceeds the wavelength of the light being used, resulting in a significant extension of the near-field region. Notably, the distance is influenced by the electrical aperture of the system rather than the physical size of the device. This characteristic makes it essential to carefully consider how to operate and control EM waves within this region. For an array of side length D, operating at a design wavelength of λ, the boundary of the far-field d_F is given by

$$d_F = \frac{2D^2}{\lambda}. \tag{1}$$

For a transmitter (Tx) and receiver (Rx) equipped with a $D_1 \times D_1$ and $D_2 \times D_2$ array, respectively, d_F is given as [16]

$$d_F = \frac{4(D_1 + D_2)^2}{\lambda}. \tag{2}$$

Hence, when the link distance is less than the far-field boundary, the fundamental regime of operation is the near-field.

To provide a clearer understanding of the near-field region, we will illustrate this concept with an example from the literature. The authors in [17] proposed a scalable and compact antenna array featuring sub-wavelength antenna spacing. This design comprises a series of hybrid plasmonic nanoantennas operating at a wavelength of 1550 nm, with configurations including 1×8 and 8×8 antenna arrays. In the case of the 8×8 array, the effective dimension is $D = 8680$ nm, calculated as 8 elements multiplied by an element spacing of 1085 nm. For an array employed at the Tx side, d_F is approximately 97 μm. If the same array configuration is employed on both the Tx and Rx sides, d_F increases to approximately 777 μm. These results underscore the significance of studying near-field intra-body optical communication, particularly as the presence of the array extends the near-field region. Changing the number of elements in the array will influence the size of the near-field region (assuming fixed antenna spacing), allowing for greater flexibility in the system design as can be seen in Fig. 1. In applications like monitoring cancer cells' response to drugs and assessing chemoresistance at the single-cell level,

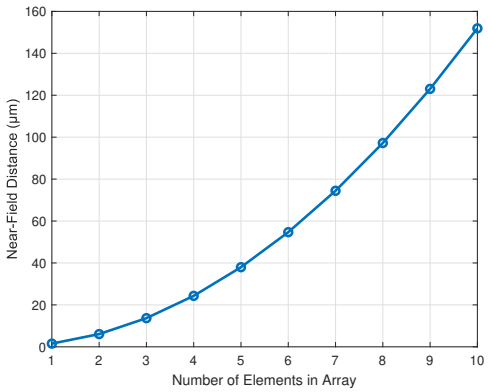

Fig. 1: Effect of antenna array elements on near-field region assuming either transmit or receive array and fixed spacing.

the working distances are typically on the order of micrometers when interacting with highly focused light sources, such as those from near-field optical techniques. This makes near-field communication particularly well-suited for precise, localized interactions with individual cells and subcellular structures, such as ion channels and receptors.

As such, using arrays provides the ability to control beam shape and direct energy with precision. This is particularly useful in intra-body communication, where spatial selectivity is important, but high power is not required, unlike in other macroscale wireless applications. Each element in the array can operate at lower power, reducing overall energy consumption while maintaining system performance.

B. Focusing an Array to the Near-Field

To focus a nanoantenna array into the near-field region, the phase of each antenna element within the array must be meticulously controlled. This is achieved by adjusting the aperture distribution of the array. For a linear array positioned along the x-axis, the aperture distribution is defined as [18]

$$f(x) = E_o(x) \exp\left(jk\frac{x^2}{2F}\right), \tag{3}$$

where $E_0(x)$ is the illumination amplitude distribution across the array, k is the wave number, x is the position along the array, and F is the focal distance. The quadratic phase shift introduced by the exponential term in (3) is analogous to the effect of a lens in traditional optics, where each point on the lens surface imparts a specific phase shift to incoming light to focus it at a particular distance.

When the phase is adjusted as in (3), the properties of the electric field in the focal plane is exactly the same as those in the far-field (for the unfocused case) [19]. As such, from array theory, several key properties of the beam can be derived based on the aperture distribution and array parameters. For a linear array with uniform feeding, the half-power beamwidth (HPBW) is approximately given [18]

$$HPBW \approx 0.88\frac{\lambda}{D}. \tag{4}$$

A larger array width D results in a narrower beam (smaller HPBW), enhancing the beam's directionality and focusing capability. When the array is focused using the aperture distribution $f(x)$, the beam width between the 3-dB points in the focal plane, known as the lateral spot size Δ_l, can be expressed as [20]

$$\Delta_l = 0.88F\frac{\lambda}{D}. \tag{5}$$

The axial spot size Δ_a, which refers to the beam's length along the propagation direction where the intensity remains above half its maximum value, is given by [20]

$$\Delta_a = 7\lambda\left(\frac{F}{D}\right)^2. \tag{6}$$

The relationship between the aperture size D and the beamwidth allows for precise manipulation of the focus and the overall beam quality. While beam focusing techniques converge at a specific focal point to achieve peak intensity, this convergence comes at the cost of rapid divergence beyond the focus, which limits the effective range of the beam. In addition, the concentration of energy into a small spot makes beam focusing highly sensitive to blockages and misalignment. Therefore, to overcome the limitations of beam divergence and sensitivity to misalignment, further exploration of alternative techniques is required.

C. Bessel Beams

Unlike traditional beams, Bessel beams arise as a candidate solution for near-field intra-body communication. In fact, Bessel beams, which are solutions to the Helmholtz equation, were first demonstrated as light fields in 1987 [21]. These beams are localized and generated through the superposition of plane waves with conically propagating wave vectors. The nth-order Bessel beam can be expressed in cylindrical coordinates [10]

$$E(r,\varphi,z) = A_0 e^{ik_z z} J_n(k_r r) e^{in\phi}, \tag{7}$$

where r, ϕ, and z are the radial, azimuthal, and longitudinal components, respectively. A_0 is the electric field amplitude, J_n is the nth-order Bessel function of the first kind, k_z and k_r are the longitudinal and radial wave vectors, respectively, with $k = \sqrt{k_r^2 + k_z^2} = 2\pi/\lambda$. Similar to a true plane wave, a perfect Bessel beam would require infinite energy over an infinite space, making its precise realization impossible. Hence, finite aperture approximations to Bessel beams can be realized using various optical elements including annular slits, axicons, metasurfaces, holograms, and arrays [22]. Specifically, the concept of using an array to generate localized waves is not new; it has been employed with both localized acoustic waves [23] and EM waves [24]. In addition to their non-diffracting nature, Bessel beams possess another crucial property: self-reconstruction, also known as self-healing. When an object obstructs the center of the beam, the waves can bypass the obstruction, creating a temporary shadow in the beam. The beam eventually restores its original intensity profile beyond the obstacle. The distance required for this self-reconstruction is given by [10].

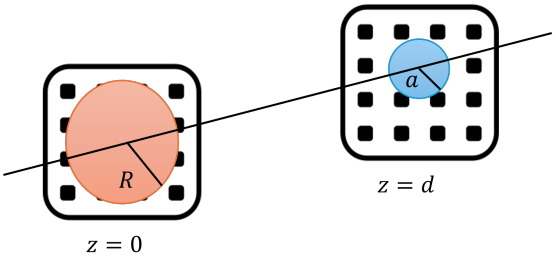

Fig. 2: System model with nanoantenna arrays at the plane $z = 0$ and $z = d$.

$$z_{min} \approx \frac{ak}{2k_z}, \tag{8}$$

where a is the width of the obstruction.

III. Bessel Beams for Intra-body Communication

A. System Model

Optical nano-antenna arrays, similar to their RF counterparts, function based on the principle of reciprocity [6]. In our proposed system, the nanoantenna array, which transmits Bessel beams as shown in Fig. 2, can be deployed at the Tx, Rx, or both, depending on the application. During transmission, the array acts as an actuator, while during reception, it functions as a detector that captures EM radiation. These arrays can also be employed for reflection, seamlessly combining both transmission and reception capabilities [6]. We focus on light propagation through blood vessels, where the nanoantennas operate at a wavelength of 1550 nm. This wavelength lies within the biological transparency window, typically spanning from about 600 nm to 1300 nm and extending from 1500 nm to 1800 nm [25]. The transparency window is characterized by reduced absorption and scattering, which allows for deeper tissue penetration and enhanced optical signal transmission.

1) Transmitter:: The transmitting nanoantenna array operates at optical frequencies, utilizing plasmonic effects to enhance the emission of a Bessel beam. This beam is generated from an aperture of radius R located in the plane $z = 0$, as illustrated in Fig. 2. The choice of aperture size is critical for determining the beam's spatial properties. A properly sized aperture ensures that the emitted Bessel beam retains its unique non-diffracting characteristics, allowing it to propagate over extended distances without significant divergence.

2) Receiver:: The receiving nanoantenna array is designed to resonate at the same optical frequency as the transmitted signal, maximizing its absorption efficiency. A disk of radius a is situated in the plane $z = d$, as shown in Fig. 2, defining the area over which the intensity of the incoming Bessel beam is integrated. This configuration enables the receiving array to capture the Bessel beam within the specified disk region.

3) Channel Characterization: We assume light propagation between the nanoantenna arrays occurs within blood vessels at 1550 nm. At this wavelength, the absorption coefficient of

blood is approximately $\mu_a \approx 5$ mm^{-1} [26]. In fact, above 1360 nm, the absorption of red blood cells (RBCs) closely follows the water absorption curve, but with values 20 to 30% lower due to minimal hemoglobin absorption, which reduces μ_a as water content decreases. In addition, for wavelengths above 600 nm, the reduced scattering coefficient μ_s' ranges from 1.8 mm^{-1} and decreases to about 1 mm^{-1} at 1550 nm [26]. The refractive index of blood at this wavelength is approximately 1.31 to 1.37 [27], varying with hemoglobin concentration, while the average RBC diameter is 7.5 μm.

B. Mathematical Formulation

In our system, we consider a zeroth-order Bessel beam ($n = 0$). The propagation occurs in the plane $z = 0$, and the electric field is given by [10]

$$E(r, z = 0) = \begin{cases} A_0 J_0(k_r r), & \text{for } r < R, \\ 0, & \text{for } r \geq R, \end{cases} \tag{9}$$

In addition, the intensity of the Bessel beam is proportional to the square of the electric field and is thus given by

$$I(r) = |E(r)|^2 = |A_0|^2 |J_0(k_r r)|^2. \tag{10}$$

The total power carried by the beam is the integral of the intensity over the entire cross-sectional area A given as [28]

$$P_t = \int_A I(r)\, dA = \frac{c}{2\pi} A_0^2 \left(\frac{R}{k_r}\right). \tag{11}$$

To derive (11), it is assumed that the aperture radius R is much larger than the central spot ($R \gg \frac{1}{k_r}$).

To fully leverage near-field wavefronts like Bessel beams, it is essential to re-evaluate key aspects of system design. In typical far-field scenarios, the Friis equation is used to calculate link budgets. However, in the near-field, the received power does not necessarily follow the $1/r^2$ decay due to wavefront spreading [29]. Instead, it becomes essential to calculate the radiated field using a diffraction integral formulation of the Huygens-Fresnel principle [29]. Given the intra-body losses at optical frequencies, the expression for power transfer becomes

$$\frac{P_r}{P_t} = \frac{\iint |E_2(x_2, y_2, d)|^2 dS_r}{\iint |E_1(x_1, y_1, 0)|^2 dS_t} \times \exp\left(-\alpha d\right), \tag{12}$$

where E_1 is the field at the Tx plane, E_2 is the field at the Rx plane, and the integrals are performed over the Rx and Tx apertures, S_r and S_t respectively. The term α represents the losses due to scattering and absorption at optical frequencies.

Due to the finite size of the nano-antenna array, which effectively acts as the aperture of the system, the generated Bessel beam has a limited propagation range. This range, denoted as z_{max}, is determined by R and the ratio of the total wave vector k to the radial wave vector k_r. The expression for the maximum propagation distance is [28]

$$z_{max} = R\sqrt{\left(\frac{k}{k_r}\right)^2 - 1}. \tag{13}$$

The condition $k > k_r > 2\pi/R$ ensures that the Bessel beam has a sufficient radial confinement relative to the aperture size. If k_r is too small or too large, or if k is too close to k_r, the beam will start to spread due to diffraction.

Finally, in the design and analysis of nanoantenna arrays, the precise control of the beam's geometry is paramount for efficient EM interaction and power transfer. Two critical parameters that define the Bessel beam's geometry are the apex angle (θ) and the spot size (r_0). The apex angle of the Bessel beam is determined by the relationship between its radial and axial wave vector components as follows [10]

$$\theta = \tan^{-1}\left(\frac{k_r}{k_z}\right). \tag{14}$$

The spot size of the central lobe, representing the radius at which the first dark ring appears around the bright central maximum, is given by [10]

$$r_0 = \frac{2.405}{k_r}. \tag{15}$$

IV. Results

In this section, we investigate the propagation characteristics of Bessel and Gaussian beams within a blood vessel. We consider a nanoantenna array capable of transmitting signals at 1550 nm to reach a target located 200 μm away. The setup includes an obstacle between the Tx and the target. The obstruction is a circular, disk-shaped region introduced into the propagation path of the beam, positioned along the z-axis at a distance of 100 μm from the beam source. This region effectively blocks the beam intensity within its spatial boundary. In biological scenarios, this obstacle can represent clusters of cells that create barriers or pathological entities, such as tumors. The simulation calculates the intensity distribution of both beams with the parameters given in Table I.

TABLE I: Simulation Parameters

Parameter	**Value**
Wavelength (λ)	1550 nm
Propagation Distance	200 μm
Beam Waist (Gaussian)	30 μm
Obstacle width (a)	20 μm
apex angle (θ)	0.88°

Figure 3(a) illustrates that the Bessel beam, even when partially obstructed, successfully reconstructs its original intensity distribution after a certain propagation distance, effectively "healing" the shadow cast by the obstacle. In our case, z_{min} is approximately 10 μm. Since the obstacle is located at 100 μm, the self-healing occurs at 110 μm as shown in Fig. 3(a). This self-healing phenomenon occurs due to the non-diffracting nature of Bessel beams, which enables them to preserve their energy distribution even in the presence of obstructions. In contrast, the Gaussian beam shows a significant drop in intensity after encountering the obstacle, and this reduction continues as it propagates further, as demonstrated in Fig. 3(b). This highlights the Gaussian beam's susceptibility to propagation effects, resulting in diminished signal strength and reduced effective range.

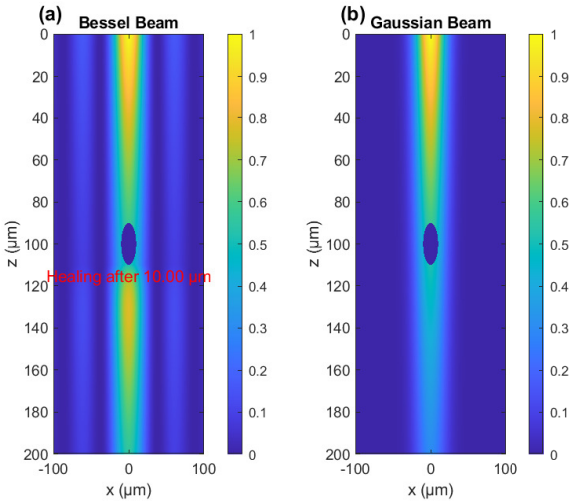

Fig. 3: Comparison between (a) Bessel and (b) Gaussian beams. Self-healing for the obstacle occurs at 110μm.

The results emphasize the practicality of using Bessel beams for near-field intra-body optical communication, where maintaining signal integrity is crucial. Their resilience makes them a compelling choice for enhancing communication efficiency between nanoantenna arrays, ensuring reliable transmission of optical signals even in complex tissue environments.

V. Conclusion

In this paper, we introduce the concept of using Bessel beams for intra-body optical communication, leveraging their distinctive properties to improve signal transmission. Our results demonstrate that Bessel beams outperform Gaussian beams, particularly in their ability to restore intensity after encountering obstacles. This self-healing feature is especially vital in intra-body applications, where tissues and cellular structures may obstruct the light path. By ensuring reliable communication channels, Bessel beams stand out as a candidate solution for various intra-body applications, including targeted therapy, bio-sensing and optogenetics. In future work, one aspect we intend to investigate is comparing the photothermal effects of both beams.

References

[1] V. Giannini, A. I. Fernández-Domínguez, S. C. Heck, and S. A. Maier, "Plasmonic nanoantennas: fundamentals and their use in controlling the radiative properties of nanoemitters," *Chemical reviews*, vol. 111, no. 6, pp. 3888–3912, 2011.

[2] D. K. Gramotnev and S. I. Bozhevolnyi, "Plasmonics beyond the diffraction limit," *Nature photonics*, vol. 4, no. 2, pp. 83–91, 2010.

[3] L. Lin and Y. Zheng, "Optimizing plasmonic nanoantennas via coordinated multiple coupling," *Scientific reports*, vol. 5, no. 1, p. 14788, 2015.

[4] S. Lal, S. Link, and N. J. Halas, "Nano-optics from sensing to waveguiding," *Nature photonics*, vol. 1, no. 11, pp. 641–648, 2007.

[5] S. Gigan *et al.*, "Roadmap on wavefront shaping and deep imaging in complex media," *Journal of Physics: Photonics*, vol. 4, no. 4, p. 042501, 2022.

[6] A. Sangwan and J. M. Jornet, "Beamforming optical antenna arrays for nano-bio sensing and actuation applications," *Nano Communication Networks*, vol. 29, p. 100363, 2021.

[7] H. Guo, P. Johari, J. M. Jornet, and Z. Sun, "Intra-body optical channel modeling for in vivo wireless nanosensor networks," *IEEE transactions on nanobioscience*, vol. 15, no. 1, pp. 41–52, 2015.

[8] A. Sangwan, H. Pandey, P. Johari, and J. M. Jornet, "Increasing the communication distance between nano-biosensing implants and wearable devices," in *2018 IEEE 19th International Workshop on Signal Processing Advances in Wireless Communications (SPAWC)*. IEEE, 2018, pp. 1–5.

[9] J. M. Jornet, V. Petrov, H. Wang, Z. Popović, D. Shakya, J. V. Siles, and T. S. Rappaport, "The evolution of applications, hardware design, and channel modeling for terahertz (THz) band communications and sensing: Ready for 6G?" *Proceedings of the IEEE*, 2024.

[10] D. McGloin and K. Dholakia, "Bessel beams: diffraction in a new light," *Contemporary physics*, vol. 46, no. 1, pp. 15–28, 2005.

[11] D. McGloin, V. Garces-Chavez, H. Melville, G. Spalding, W. Sibbett, and K. Dholakia, "Advanced micromanipulation using Bessel beams," in *2003 Conference on Lasers and Electro-Optics Europe (CLEO/Europe 2003)(IEEE Cat. No. 03TH8666)*. IEEE, 2003, p. 710.

[12] X. Ge, S. Chen, S. Chen, and L. Liu, "High resolution optical coherence tomography," *Journal of Lightwave Technology*, vol. 39, no. 12, pp. 3824–3835, 2021.

[13] S. Li and J. Wang, "Adaptive free-space optical communications through turbulence using self-healing Bessel beams," *Scientific reports*, vol. 7, no. 1, p. 43233, 2017.

[14] I. V. Reddy, D. Bodet, A. Singh, V. Petrov, C. Liberale, and J. M. Jornet, "Ultrabroadband terahertz-band communications with self-healing bessel beams," *Communications Engineering*, vol. 2, no. 1, p. 70, 2023.

[15] E. F. Knott, J. F. Schaeffer, and M. T. Tulley, *Radar cross section*. SciTech Publishing, 2004.

[16] V. Petrov, J. M. Jornet, and A. Singh, "Near-field 6G Networks: Why Mobile Terahertz Communications MUST Operate in the Near Field," in *GLOBECOM 2023 - 2023 IEEE Global Communications Conference*, 2023, pp. 3983–3989.

[17] Y. Xu, T. Dong, J. He, and Q. Wan, "Large scalable and compact hybrid plasmonic nanoantenna array," *Optical Engineering*, vol. 57, no. 8, pp. 087 101–087 101, 2018.

[18] A. Badawi, A. Sebak, and L. Shafai, "Array near field focusing," in *IEEE WESCANEX 97 Communications, Power and Computing. Conference Proceedings*, 1997, pp. 242–245.

[19] J. Sherman, "Properties of focused apertures in the Fresnel region," *IRE Transactions on Antennas and Propagation*, vol. 10, no. 4, pp. 399–408, 1962.

[20] W. Graham, "Analysis and synthesis of axial field patterns of focused apertures," *IEEE transactions on antennas and propagation*, vol. 31, no. 4, pp. 665–668, 1983.

[21] J. Durnin, J. Miceli Jr, and J. H. Eberly, "Diffraction-free beams," *Physical review letters*, vol. 58, no. 15, p. 1499, 1987.

[22] P. Lemaitre-Auger, S. Abielmona, and C. Caloz, "Generation of Bessel beams by two-dimensional antenna arrays using sub-sampled distributions," *IEEE transactions on antennas and propagation*, vol. 61, no. 4, pp. 1838–1849, 2012.

[23] J. Hernandez, R. Ziolkowski, and S. Parker, "Synthesis of the driving functions of an array for propagating localized wave energy," *The Journal of the Acoustical Society of America*, vol. 92, no. 1, pp. 550–562, 1992.

[24] R. W. Ziolkowski, "Properties of electromagnetic beams generated by ultra-wide bandwidth pulse-driven arrays," *IEEE transactions on antennas and propagation*, vol. 40, no. 8, pp. 888–905, 1992.

[25] C. Li and Q. Wang, "Challenges and opportunities for intravital near-infrared fluorescence imaging technology in the second transparency window," *ACS nano*, vol. 12, no. 10, pp. 9654–9659, 2018.

[26] M. Friebel, J. Helfmann, U. Netz, and M. Meinke, "Influence of oxygen saturation on the optical scattering properties of human red blood cells in the spectral range 250 to 2000 nm," *Journal of biomedical optics*, vol. 14, no. 3, pp. 034 001–034 001, 2009.

[27] E. N. Lazareva and V. V. Tuchin, "Measurement of refractive index of hemoglobin in the visible/NIR spectral range," *Journal of biomedical optics*, vol. 23, no. 3, pp. 035 004–035 004, 2018.

[28] J. Durnin, J. Miceli, and J. H. Eberly, "Comparison of Bessel and Gaussian beams," *Optics letters*, vol. 13, no. 2, pp. 79–80, 1988.

[29] H. Guerboukha, B. Zhao, Z. Fang, E. Knightly, and D. M. Mittleman, "Curving THz wireless data links around obstacles," *Communications Engineering*, vol. 3, no. 1, p. 58, 2024.